



# Impacts of the land use and land-cover changes on local hydroclimate in southwestern Amazon

Isabel L. Pilotto<sup>1</sup> · Daniel A. Rodriguez<sup>2</sup> · Sin-Chan Chou<sup>1</sup> · Lucas Garofolo<sup>3</sup> · Jorge L. Gomes<sup>1</sup>

Received: 2 September 2022 / Accepted: 24 June 2023 / Published online: 3 July 2023  
© The Author(s), under exclusive licence to Springer-Verlag GmbH Germany, part of Springer Nature 2023

## Abstract

This paper investigates the effects of advancing deforestation in the southwestern Amazon on local hydroclimate. For this purpose, a high-resolution mesoscale model, coupled with a land surface model and a hydrologic routing model, is integrated for five years in two experiments, one control without changes in land use and another changing land use annually. During the rainy season, simulated higher precipitation volumes are reduced with the expansion of pasture lands. In the dry periods, mainly in August, there is an increase in precipitation over some deforested areas, which can be associated with mesoscale circulations induced by the heterogeneous surface. In general, land-use changes reduce evapotranspiration and the net radiation at the surface and increase the sensible heat flux during the dry season. In the rainy period, there is an increase in evapotranspiration with the intensification of deforestation, which modifies the other components of energy balance. Results suggest that the impact of LUCC on the local climate is more affected by conditions that generate precipitation extremes (El Niño/La Niña events) than by the abrupt increase in the annual deforestation rate. Land-use changes reduce the streamflow in all sub-basins of Ji-Parana during the dry season. In the rainy season, LUCC increases the streamflow during periods with normal precipitation conditions and La Niña in almost all sub-basins, except in the sub-basin with more than 20% deforestation.

**Keywords** Deforestation · Land use and land cover modeling · Hydroclimate · Streamflow · Amazonia

## 1 Introduction

The Brazilian Amazonia has already lost almost 20% of its original forest cover (INPE 2022a). According to the Terra-Class data (INPE 2022b), approximately 60% of this deforested area was converted to pasture. The state of Rondonia has the highest percentage, with 79% of the deforested area converted to pasture (Almeida et al. 2016). Land use and land-cover changes (LUCC) affect the hydroclimatic

processes via changes in the energy and water balances (e.g., D’Almeida et al. 2007; Nobre et al. 1991).

The increase in surface albedo due to deforestation causes a reduction in solar radiation absorbed by the surface. Leaf area index (LAI) and the rooting depth decrease with the removal of the forest, which contributes to diminishing evapotranspiration rates. The increased near-surface air temperature caused mainly by the reduction in evapotranspiration generates an enhancement in longwave radiation emitted by the surface. Consequently, net radiation at the surface resulting from the surface radiation balance decreases with deforestation. Latent heat flux decreases with the reduction in evapotranspiration, while sensible heat flux increases due to the increased surface temperature. These results have been found in some modeling and observational studies about the impacts of the LUCC on climate in Amazonia (e.g., Findell et al. 2007; Costa and Foley 2000; Pilotto et al. 2017; Rodriguez et al. 2014; von Randow et al. 2004).

Discrepancies found in different numerical studies are mainly related to the type of numerical model, the spatial

✉ Isabel L. Pilotto  
isabel.pilotto@inpe.br; isabelpilotto@gmail.com

<sup>1</sup> Center for Weather Forecasting and Climate Studies (CPTEC), National Institute for Space Research (INPE), Cachoeira Paulista, Brazil

<sup>2</sup> Alberto Luiz Coimbra Institute for Graduate Studies and Research in Engineering - COPPE, Federal University of Rio de Janeiro, Rio de Janeiro, Brazil

<sup>3</sup> Earth System Science Center (CCST), National Institute for Space Research (INPE), São José dos Campos, Brazil

scale of deforestation, and the period of the annual cycle of precipitation. General circulation models (GCMs) generally have a coarse spatial resolution, between 1° and 3°, and adopt large-scale deforestation to produce some response. Modeling studies using coarse resolutions, which considered large-scale deforestation in the Amazonia, generally have found a reduction in both evapotranspiration and precipitation rates (e.g., Costa and Foley 2000; Nobre et al. 1991; Pitman and Lorenz 2016; da Silva et al. 2008; Lejeune et al. 2015). This reduction of precipitation is the result of the average over the whole Amazon Basin, which shows a dipole pattern with a larger area of reduction in the northwest of the basin and a smaller area of increased precipitation in the southeast of the basin (e.g., Lejeune et al. 2015; Medvigy et al. 2011).

Regional climate models (RCMs) can provide a more refined surface representation, capturing small forest clearings. Therefore, many numerical experiments using RCMs models with small-scale deforestation have simulated increased precipitation over deforested areas. This increased precipitation is generally associated with local circulations induced by surface heterogeneities (e.g., Baidya Roy and Avissar 2002; Chagnon and Bras 2005; Negri et al. 2004; Wang et al. 2000, 2009).

Baidya Roy (2009) states that warmer temperatures over deforested areas create horizontal pressure gradients, forcing cool, moist air from adjacent forests to converge over the clearings. The increased convergence can trigger shallow cumulus clouds and produce precipitation over the deforested patches (e.g., Baidya Roy 2009; Baidya Roy et al. 2002; Chagnon and Bras 2005; Wang et al. 2009). This mechanism, called “vegetation breezes” by Baidya Roy (2009), is commonly found in the Brazilian State of Rondonia, in the southwestern Amazon, which has a characteristic pattern of fragmentation so-called fishbone with a scale on the order of 10 km (Arima et al. 2016; de Oliveira Filho and Metzger 2006). Khanna et al. (2017) found an increase in cloudiness over the small-scale deforestation patches in the 1980s in Ji-Paraná through satellite images. This process of vegetation breezes found over the fishbone patches in Rondonia has occurred more frequently in the dry season (e.g., Chagnon et al. 2004; Chagnon and Bras 2005; Wang et al. 2009; Baidya Roy 2009).

Regional modeling studies at higher spatial resolutions over the fishbone patches in Rondonia have also found an increase in cloudiness and precipitation (e.g., Baidya Roy 2009; Wang et al. 2000). However, the temporal scales of these studies are short, corresponding to specific case studies. Changes in the surface characteristics and heterogeneity can modify feedback processes between the land surface and atmosphere within months or even years (Guillod et al. 2015; Koster et al. 2004; Seneviratne et al. 2006). Therefore,

numerical model runs are necessary at higher spatial resolutions and long-term integrations to assess the LUCC effects more appropriately.

Generally, most modeling studies of LUCC impact do not include time series of LUC change into the integration; instead, they compare two integrations with different land cover and land use to evaluate the impacts. This way is not possible to know how the climate responds continuously to the advance of deforestation. Also, changes in the hydrological response, driven by these local climate changes, have a slow and time-lagged response, mainly because of the large memory in soil processes.

Therefore, the objective of this work is to assess the hydroclimatic local response to the annual expansion of deforestation over the Ji-Paraná Basin in Rondonia using a coupled atmosphere-land surface-river routing model, at 1-km resolution, for 5-year period time integrations (1984–1989), with yearly updates of the LUCC. Although deforestation over the region in the 1980s is lower in terms of km<sup>2</sup> compared to the present day, its annual deforestation rates are the highest ever mapped by the Prodes (e.g., Linhares 2005).

## 2 Materials and methods

The three components of the coupled atmosphere – land surface – river routing modeling system used in this study are briefly described. The experiment setup is explained.

### 2.1 Eta model

The Eta model (Mesinger et al. 2012) is a grid-point model that uses the eta vertical coordinate defined by Mesinger (1984) and represents the topography in cut-cells. The parameterization schemes used in the Eta model for this study are: the Betts–Miller–Janjić (Janjić 1994) for cumulus convection; the Zhao scheme (Zhao and Carr 2002) for cloud microphysics; the Geophysical Fluid Dynamics Laboratory package of shortwave (Lacis and Hansen 1974) and longwave (Fels and Schwarzkopf 1975) radiation schemes; and the Mellor–Yamada level 2.5 level (Mellor and Yamada 1982) for the atmospheric turbulence. Pilotto et al. (2017) replaced the Noah Land Surface Model (LSM) (Ek et al. 2003) with the Noah-Multiparameterization (Noah-MP) LSM (Niu et al. 2011) to represent the land surface in the Eta model. This version is now referred to as Eta/Noah-MP, and it is described in more detail in the next section.

The Eta model has been used for various applications, such as: for seasonal hindcasts (e.g. Chou et al. 2005; Pilotto et al. 2012; Chou et al. 2020), for land use and land cover change impact studies (e.g., Correia et al. 2008; Pilotto et

al. 2017; Rodriguez et al. 2014), for regional climate change projections (Pesquero et al. 2010; Chou et al. 2012, 2014; Marengo et al. 2012; Lyra et al. 2018; Resende et al. 2019), and various climate change impacts studies (Tavares et al. 2018; Imbach et al. 2018; Chou et al. 2019).

## 2.2 Noah-MP

The Noah-MP is a land surface model with multiple options to model land surface-atmosphere processes (Niu et al. 2011). The Noah-MP LSM is developed over the Noah LSM framework. This new version includes a vegetation canopy layer to compute the canopy and the ground surface temperatures separately. The Noah-MP version uses the modified two-stream radiation transfer scheme (Niu and Yang 2004; Yang and Friedl 2003) that considers canopy gaps to compute fractions of sunlit and shaded leaves and their absorbed solar radiation. Also, a semi-tile sub-grid scheme considers vegetation and bare soil in the cell grid.

In this study, we used the Jarvis scheme for canopy stomatal resistance (Jarvis 1976), the Noah-type soil moisture factor for soil moisture dynamics (Niu et al. 2011), the simple groundwater model with a runoff scheme based on TOP-MODEL (Niu et al. 2005, 2007), and the surface exchange coefficient for heat ( $C_h$ ) following Chen et al. (1997)

The Noah-MP LSM correctly reproduced the surface processes in the Amazonia region in the forest and pasture observational sites (Pilotto et al. 2015).

The Noah-MP version in this study differs from Pilotto et al. (2017) by including the change of land use and land cover map along the integration. This version also differs by adding four soil layers reaching a depth of up to 12 m, discretized in 8 soil layers. The Amazon rainforest has a deep rooting zone, which reaches about 10 m and contributes to the maintenance of evapotranspiration during the dry season (e.g., Bruno et al. 2006; da Rocha et al. 2004). A consistent update follows the annual update in the land cover map in the vegetation parameters in the model. This model development tries to more accurately reproduce the atmospheric response to land use and land cover changes.

## 2.3 River routing

Streamflow discharges in 7 gauge-stations were estimated using the hydrologic channel-flow routing model based on the Muskingum-Cunge (Cunge 1969) routing model from the MHD-INPE model (Rodriguez and Tomasella 2016). The Channel network was obtained using data from the Shuttle Radar Topography Mission with 90 m resolution (Farr and Kobrick 2000; Farr et al. 2007). Calibrated routing parameters were obtained from Rodriguez and Tomasella (2016). The authors calibrated the MHD-INPE model

using measured hydrometeorological data from 1982 to 2006. Model performance was satisfactory, with correlation coefficients between 0.66 and 0.87 (Table 2 in Rodriguez and Tomasella 2016). The input for the routing model was the surface and subsurface water excess estimated by Noah-MP. Measured streamflow data from the Brazilian National Water Agency was used to evaluate simulated water discharges.

## 2.4 Study area

The study area was delimited by the latitude coordinates 13.25°S to 10.54°S, and longitudes 63.37°W to 59.83°W (Fig. 1), which includes the Ji-Parana basin, located in the Brazilian State of Rondonia, in the Southwestern Amazon.

The natural vegetation cover of the study area includes cerrado (a type of savanna), dense forest, open forest, and semideciduous forest (Linhares 2005). Clear-cut deforestation rates in Rondonia State have been rising since the 1970s due to the construction of main road BR-364 (Alves et al. 1999, 2003; Alves 2002a, b; Arima et al. 2016) and the overwhelming land occupation policy at that time (Alves et al. 2003; Arima et al. 2016; Machado 1998; Moran 1981). The dominant pattern of land use fragmentation in the study area, especially in the central and northwestern regions, is the fishbone pattern associated with the deforested land for rural settlements (Arima et al. 2016; Linhares 2005). In the southeastern region, there are some extensive forests cleared areas for large-scale agriculture (Linhares 2005).

Köppen's climate classification for Rondonia is Am (Tropical monsoon climate). The annual climatological precipitation measured about 378 km north of Ji-Parana, is about 2,300 mm. June, July, and August are the driest months when monthly total rainfall is less than 50 mm. The wet season starts in November and ends in March, with maximum precipitation in January of about 320 mm per month (INMET 1992).

## 2.5 Experiments set-up

The Eta/Noah-MP model was configured with a 1-km horizontal resolution and 38 atmospheric layers over the black square area shown in Fig. 1. The simulations were set up in two experiments: 1) one referred to as LUCC, with a yearly update of the land use and land-cover conditions during the integration time. The other experiment was called the control experiment or CTL, with the vegetation kept constant during the integration time. Both experiments started in May 1984 through June 1989 and started with the 1983 vegetation cover information from Landsat data (Linhares 2005; Rodriguez et al. 2014). However, the land cover of the LUCC experiment was updated yearly from 1983 (Fig. 2a)

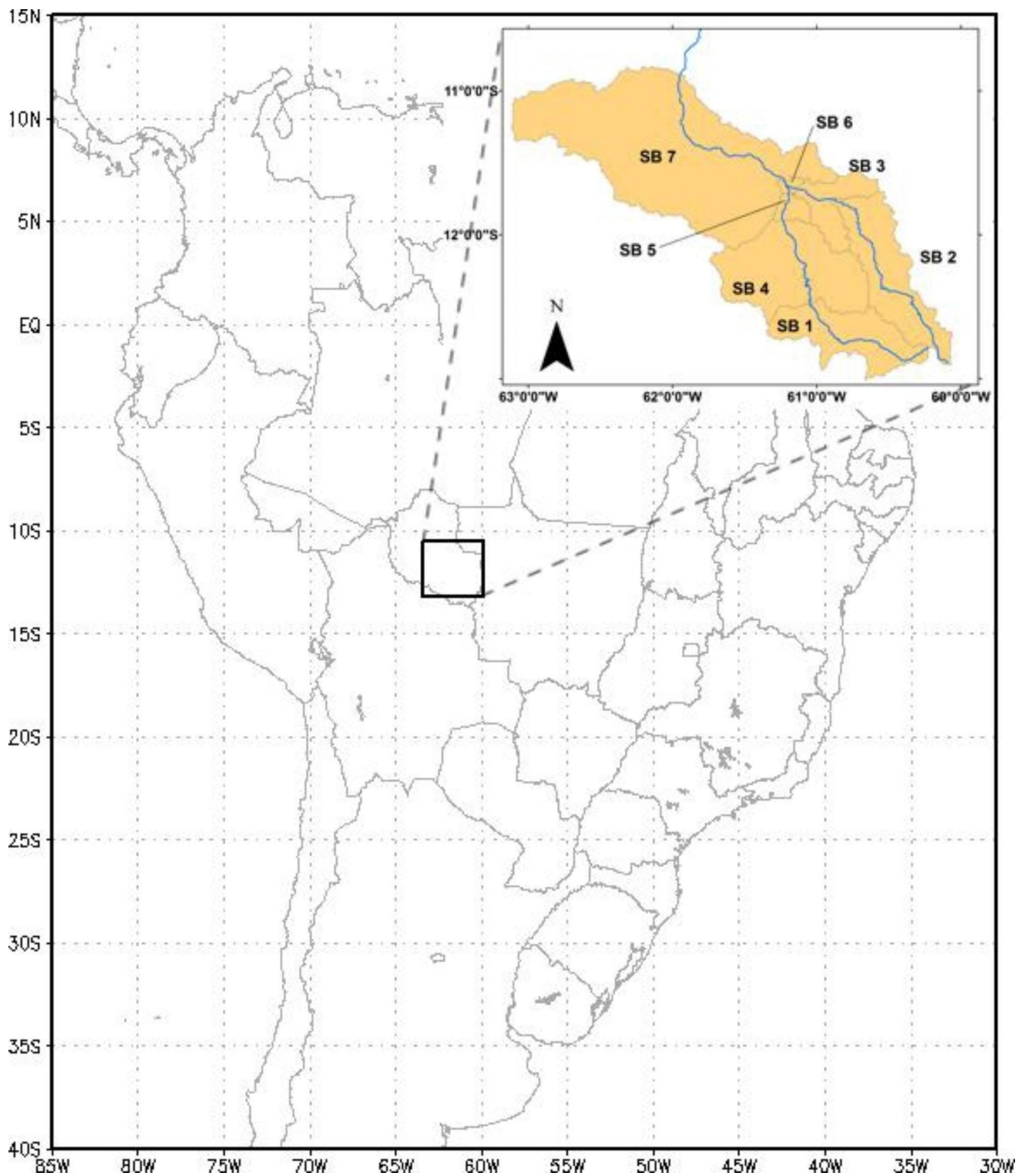
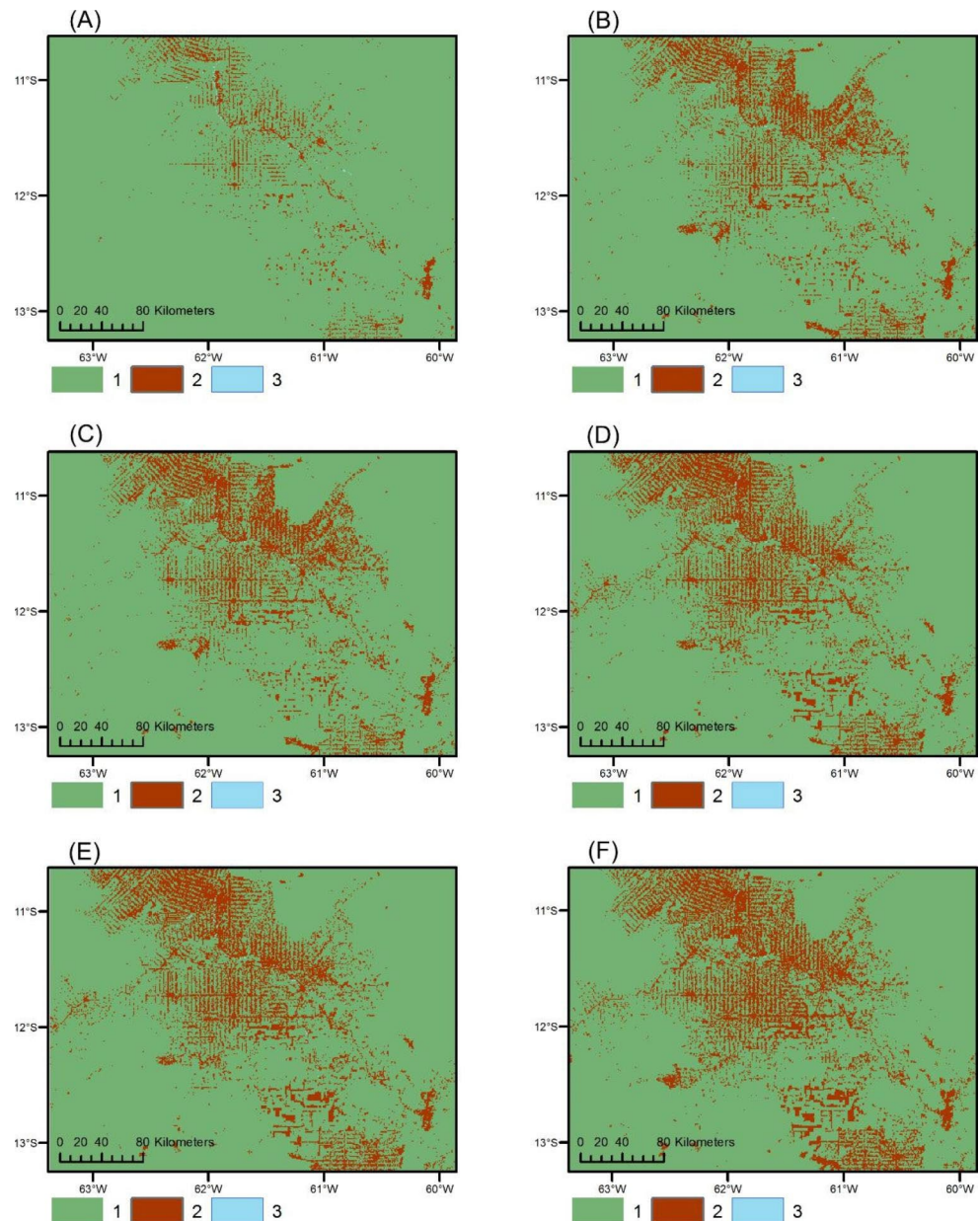


Fig. 1 South America map. The black rectangle corresponds to the area of the integration domain

to 1988 (Fig. 2f), always in August, because of the higher incidence of deforestation practices occurring at the end of the dry season (Alves 2002).

The annual deforestation rates in the Ji-Parana basin were almost 10, 4, and 5% in 1984, 1985, and 1986, respectively (Linhares 2005 and Rodriguez et al. 2010), while the rates in the 2000s did not exceed 3% (Figure S1). This higher

**Fig. 2** Land use and land cover maps from (a) 1983, (b) 1984, (c) 1985, (d) 1986, (e) 1987, (f) 1988, where green, brown, and white areas are considered forest, deforestation, and water, respectively



deforestation rate in the transition from 1983 to 1984 is related to improving the road mesh, mainly BR 364, which facilitated access to areas further away from the capital of Porto Velho (Linhares 2005). Also, Linhares (2005) suggested that the 1983 drought caused by the El Niño event may have encouraged deforestation.

Eta simulations used boundary and initial conditions downscaled from ERA-Interim reanalysis (Dee et al. 2011). Soil data are from the SOTERLAC (Dijkshoorn et al. 2005). Land use and land cover maps were obtained from Landsat data (Linhares 2005; Rodriguez et al. 2014). This dataset contains only two land use types, forest and pasture, at 30-m resolution. The vegetation parameters were modified for local characteristics (e.g., Rodriguez et al. 2014).

## 3 Results

### 3.1 Spatial pattern

The variables analyzed in spatial fields shown in Figs. 3 and 4, and 5 are precipitation, air temperature at 2 m, net radiation at the surface, and latent and sensible heat fluxes. These fields correspond to the difference in the 5-years seasonal average between the LUC and CTL experiments for the wet season, December-January-February (DJF), and the dry season, June-July-August (JJA). The solid black line in the figures is the 1988 deforested boundary (DB88), the last year land use was updated in the LUC experiment.

Spatial patterns simulated by the model show a seasonal variability in both experiments (Figures S2–S11), with maximum values ranging between the dry and rainy seasons of 6–12 mm day<sup>-1</sup> for precipitation, 26–29°C for the air temperature at 2 m, 155–215 W m<sup>-2</sup> for net radiation at the surface, 125–155 W m<sup>-2</sup> for latent heat flux, and 70–115 W m<sup>-2</sup> for sensible heat flux.

### 3.1.1 Precipitation and air temperature at 2 m

Five years-averaged precipitation from the CTL experiment has maximum values (> 12 mm day<sup>-1</sup>) in regions predominantly covered by forest (Figure S2a) in DJF, which is reduced in the LUCC experiment where many of these areas were replaced by pastures (Figure S2b). This pattern

also occurs in the dry season but with less intensity (Figures S3a,b).

The most significant differences between the LUCC and CTL experiments occur where deforestation has expanded over the years studied (Fig. 3a,b, S12). The impact of LUCC on precipitation is generally of reduction (Fig. 3a,b), especially during the rainy season, reaching 4 mm day<sup>-1</sup> (Fig. 3a).

LUCC experiment reduces precipitation by up to 2 mm day<sup>-1</sup> in the dry season over the central-northeastern region dominated by fishbone deforestation, compared with the CTL experiment (Fig. 3b). This signature of change in precipitation appears in the June and July fields (Figure S13a,b). There are also areas with increased precipitation of about 0.5–1 mm day<sup>-1</sup> over the center-northwestern of DB88 in JJA (Fig. 3b). Increased precipitation occurs predominantly

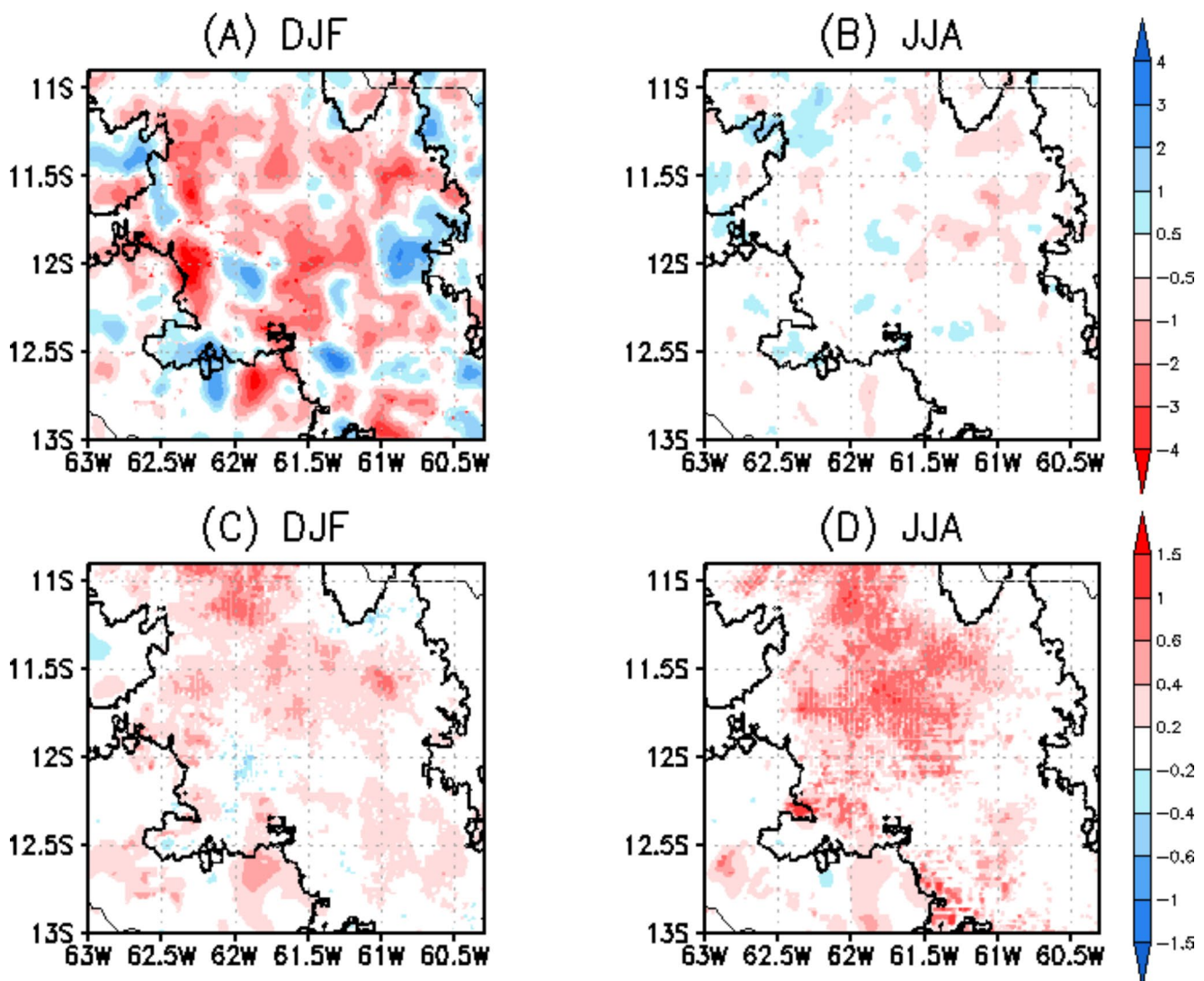


**Fig. 3** Difference of monthly precipitation (mm day<sup>-1</sup>) averaged between 1984 and 1989 from LUCC and CTL experiments in (a) DJF and (b) JJA. The difference in air temperature at 2 m (°C) averaged

between 1984 and 1989 from LUCC and CTL experiments in (c) DJF and (d) JJA. The black outlines correspond to the pasture cover from 1988

in August (Figures S13c), reaching up to  $3 \text{ mm day}^{-1}$  over the DB88. Earlier studies in the same region suggested that the fishbone shapes trigger mesoscale circulations, contributing to increased precipitation mainly during the dry season (e.g., Baidya Roy 2009; Baidya Roy et al. 2002; Chagnon and Bras 2005; Wang et al. 2009).

Accelerated deforestation produces a rise in air temperature at 2 m by more than  $1.5^\circ\text{C}$  during the DJF (Fig. 3c) and JJA (Fig. 3d) periods. However, the impact is more substantial in the dry than the rainy season, reaching more deforested lands (Figure S14). In DJF, a reduction in near-surface air temperature of about  $0.2\text{--}0.6^\circ\text{C}$  is observed in small pasture patches (Fig. 3c and S14a).

### 3.1.2 Energy fluxes

#### a. Net radiation at the surface

Land use and land cover changes reduce the net radiation at the surface by about  $20 \text{ W m}^{-2}$  in both seasons (Fig. 4). However, this impact affects more deforested lands in the dry season (Fig. 4b) than in the rainy season (Fig. 4a and S15).

Small areas with increased net radiation of  $5 \text{ W m}^{-2}$  are found over some pasture patches in DJF (Fig. 4a and S15a). This increase in net radiation at the surface with the expansion of the deforestation probably occurred due to an increase in evaporation (Fig. 5a and S16a), enough to cool the air near the surface (Fig. 3c and S14a), which decreases the longwave radiation emitted by the surface, increasing the net radiation.

#### b. Latent and sensible heat fluxes

In the rainy season, there are deforested areas where the difference between the LUCC and CTL experiments indicates an increase in latent heat flux (Fig. 5a and S16a) and a reduction in sensible heat flux of up to  $40 \text{ W m}^{-2}$  (Fig. 5c and S17a). This increase in evapotranspiration resulted in a reduction in near-surface air temperature (Figure S14a), which decreased the sensible heat flux.

In the dry season, LUCC reduces evapotranspiration (Fig. 5b and S16b) and increases sensible heat flux in most of the DB88, reaching differences of up to  $40 \text{ W m}^{-2}$  (Fig. 5d and S17b).

Notes that maximum magnitudes of latent and sensible heat flux changes are observed in the largest clearing areas,

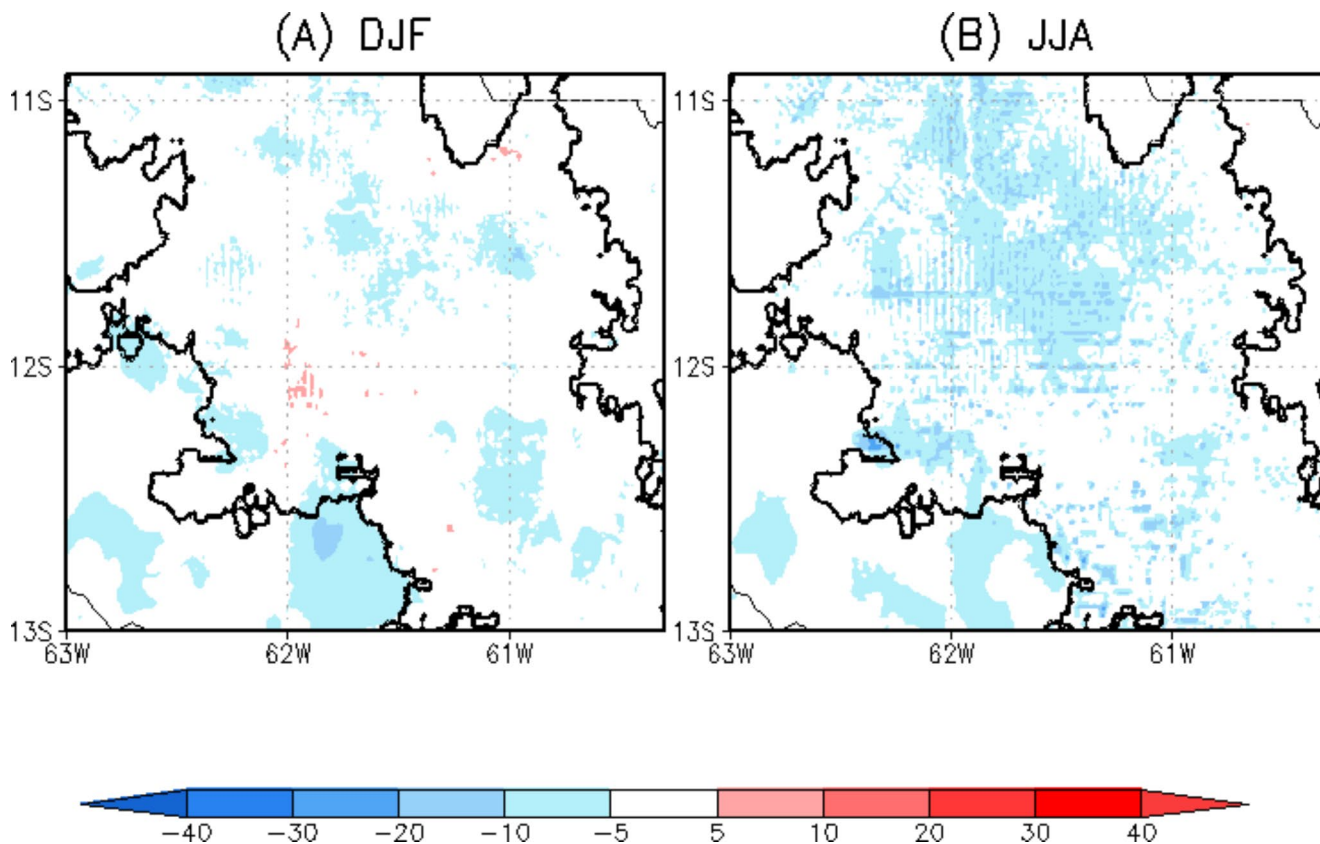


**Fig. 4** Difference of net radiation at the surface ( $\text{W m}^{-2}$ ) averaged between 1984 and 1989 from LUCC and CTL experiments in (a) DJF and (b) JJA. The black outlines correspond to the pasture cover from 1988

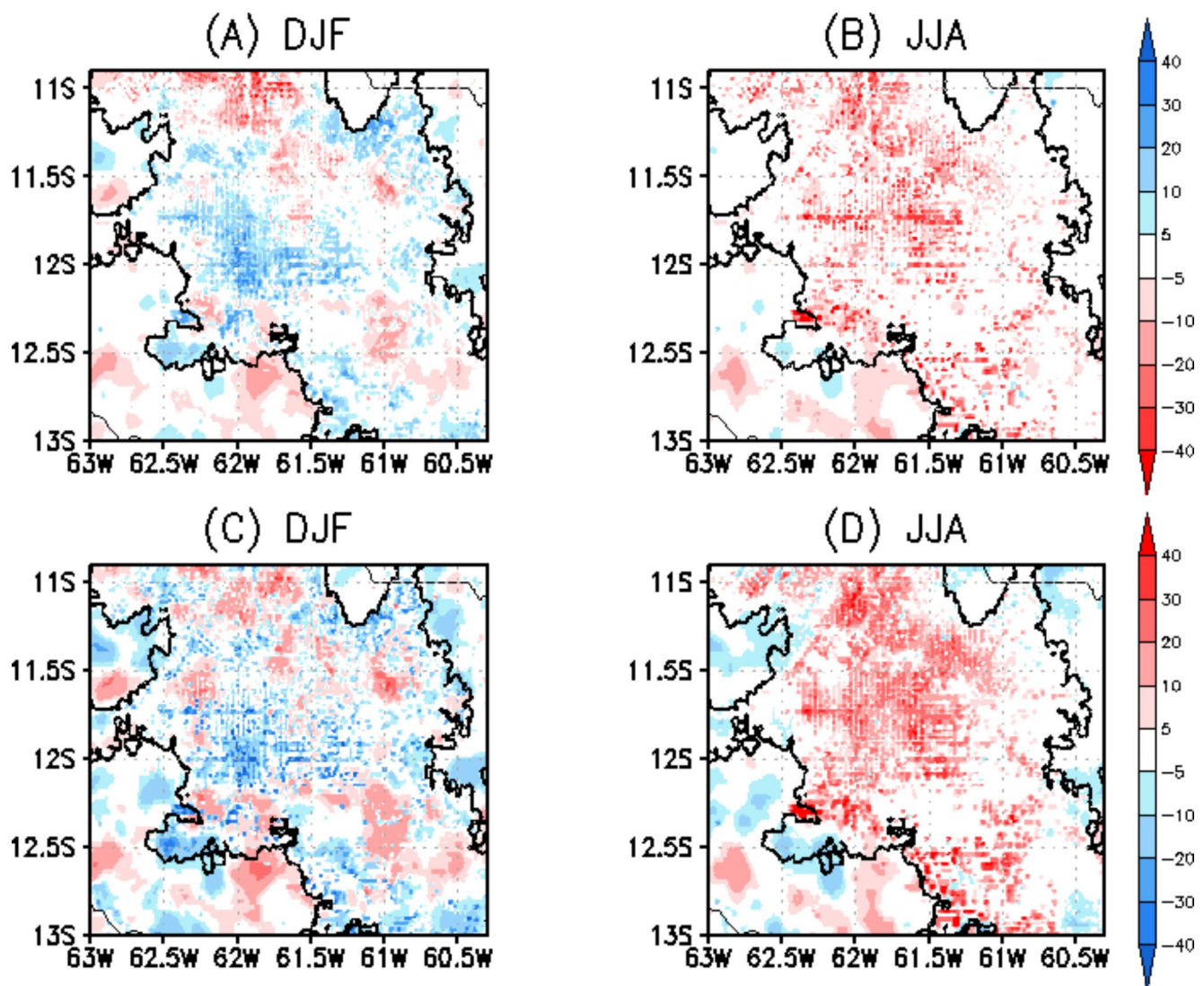


**Fig. 5** Difference of latent heat flux ( $\text{W m}^{-2}$ ) averaged between 1984 and 1989 from LUCCL and CTL experiments in (a) DJF and (b) JJA. The difference of sensible heat flux ( $\text{W m}^{-2}$ ) averaged between 1984

and 1989 from LUCCL and CTL experiments in (c) DJF and (d) JJA. The black outlines correspond to the pasture cover from 1988

dominated by large-scale agriculture, and in the fishbone pattern. For example, there is a large change in a patch ( $\sim 11.7^{\circ}\text{S}$  and  $62.3^{\circ}\text{W}$ ) that compose the fishbone pattern, which was occupied by surplus settlers from an old rural settlement (Rolim de Moura sector), and grew up in the 1980s, forming the municipality of Nova Brasilândia d'Oeste in 1987. The LUCCL experiment captures it because considers the growth of deforestation over the years, unlike the CTL experiment.

### 3.2 Interannual variability

In the previous section, the analyzes focus on the spatial patterns of hydrometeorological response to LUCCL, ignoring interannual variability. Monthly precipitation and energy

fluxes were averaged over the DB88 region for both experiments to assess interannual variability.

LUCCL and CTL experiments adequately represent the magnitude and seasonality of precipitation over the years compared to the MSWEP data (Beck et al. 2017). Precipitation from both experiments shows similar values from 1984 to 1986 (Fig. 6a). Differences reach a maximum magnitude of  $0.4 \text{ mm day}^{-1}$ . From 1987 until mid-1988, the differences between the experiments increased, showing a precipitation reduction of up to  $2 \text{ mm day}^{-1}$  from the LUCCL experiment compared with the control experiment. The moderate 1986–1987 El Niño event occurred in this period, which lasted approximately 18 months, from mid-1986 to early 1988 (Zhang and Endoh 1994). 1987 was a dry year in the region of the Ji-Parana basin (Rodríguez et al. 2010).



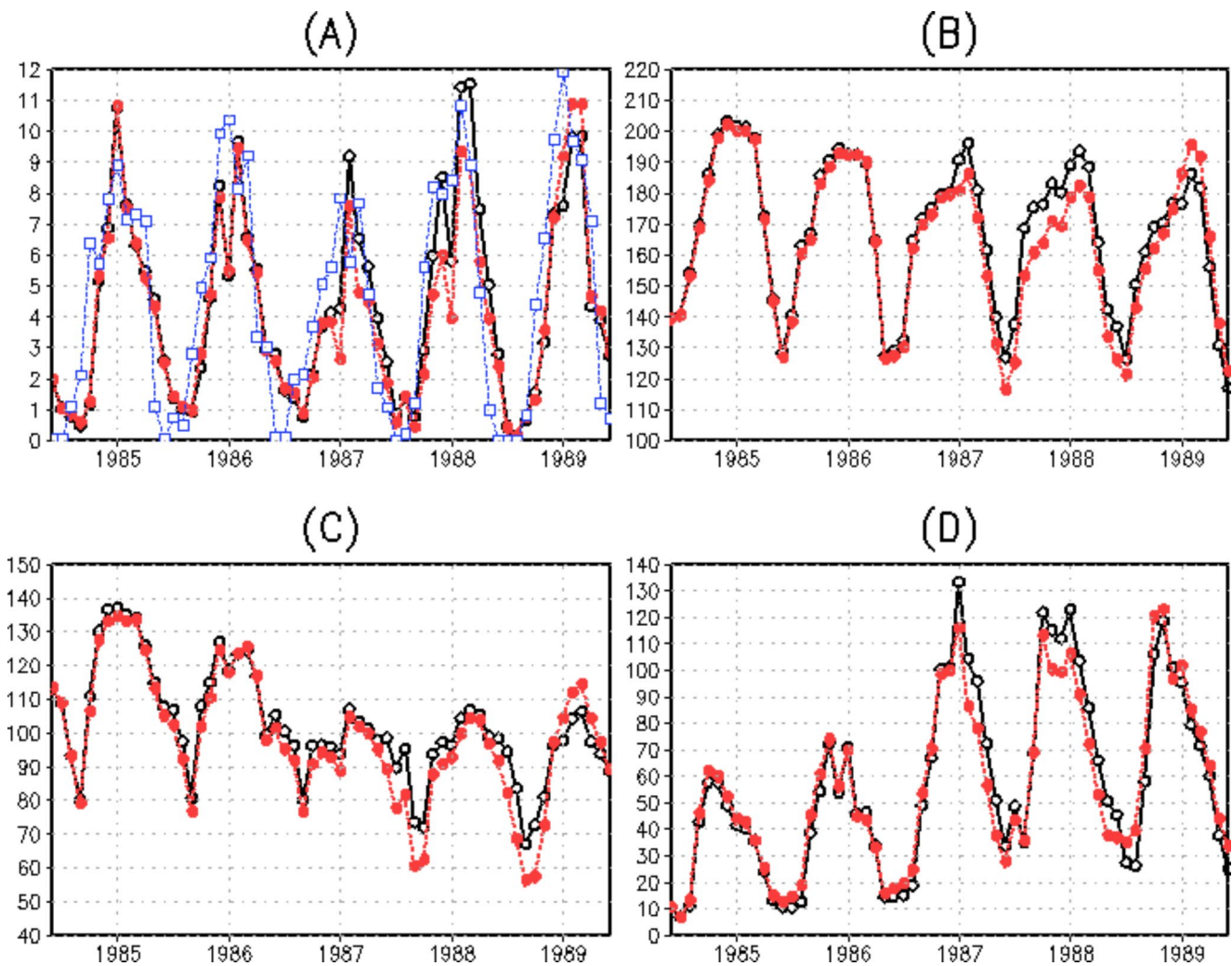


**Fig. 6** Interannual variability of (a) precipitation ( $\text{mm day}^{-1}$ ), (b) net radiation at the surface ( $\text{W m}^{-2}$ ), (c,d) latent and sensible heat fluxes ( $\text{W m}^{-2}$ ) from the LUC (red lines), and CTL (black lines) experiments,

the average for (a) the deforested area of 1988. The blue line in (a) is the precipitation ( $\text{mm day}^{-1}$ ) from the MSWEP

After this El Niño episode, a strong event of La Niña started, with its height in September 1988 (Zhang and Endoh 1994). Notes that in 1989, while acting the La Niña episode, the response of precipitation was opposite, showing an increase above  $1 \text{ mm day}^{-1}$  with the advance of deforestation (Fig. 6a). Some studies directly relate droughts (floods) events in the Amazon to El Niño (La Niña) episodes (e.g. Aceituno 1988; Uvo et al. 1998; Williams et al. 2005; Espinoza et al. 2012, 2013; Marengo and Espinoza 2016).

In general, net radiation (Fig. 6b) and latent heat flux (Fig. 6c) in the LUC experiment are smaller than in the CTL experiment until 1988. This reduction of net radiation is expected because of the increase in albedo under LUC conditions. In 1989, when precipitation was larger in LUC than in CTL, also net radiation is larger.

As observed in precipitation, the largest differences between net radiation and evapotranspiration occurred

between the experiments in 1987 and 1988 ( $\sim 10 \text{ W m}^{-2}$ ). Sensible heat flux from the LUC experiment is higher than the CTL experiment during the driest months (Fig. 6d) when soil moisture is stored at the deepest soil layers. During the driest periods, soil moisture is stored at the deepest soil layers, the skin surface is warmer, and vegetation with shallow roots, such as pastures, transpires at lower rates than forests with deeper roots (e.g., Bruno et al. 2006; Pilotto et al. 2017).

In the rainy periods of 1986, 1987, and 1988, sensible heat flux differences are also explained by soil water availability and the evapotranspiration rates under pasture and forest. Evapotranspiration, and thus heat flux partition, is controlled by soil water distribution. During these wetter periods, the soil moisture content in the shallow soil layers allows similar evapotranspiration rates (Fig. 6c) between pasture and forest (e.g., von Randow et al. 2004), thus,

because of the lower net radiation in LUCC, sensible heat flux is lower than in CTL experiment.

The land use change between 1983 and 1984, which has an annual deforestation rate of almost 10%, caused an increase of  $0.1 \text{ mm day}^{-1}$  in precipitation, of  $1.8 \text{ W m}^{-2}$  in sensible heat flux, and a reduction of  $0.3$  and  $1 \text{ W m}^{-2}$  in the latent heat flux and net radiation, respectively. This comparison was made between the LUCC and CTL experiments in August 1984, when the vegetation map was first updated.

### 3.3 Streamflow

The Eta/Noah-MP model simulates total runoff as the sum of water excess at the surface and each soil layer (Niu et al. 2011). The total runoff was routed through a network of river channels in the basin to simulate streamflow at gauge stations (Fig. 7). The streamflow shown in Figs. 7 and 8 started in October 1985 due to the beginning of the hydrological year. The simulated monthly average streamflow adequately reproduced the observed seasonal variability but did not accurately capture the discharge volumes.

These results are shown in values of  $R^2$  between poor and satisfactory (Harmel et al. 2007). The model underestimates the streamflow during wet and dry seasons, resulting in a large RMSE (Table 1).

However, as observed in precipitation and energy fluxes, the largest differences in streamflow between the experiments occur during the El Niño and La Niña episodes in most sub-basins (Fig. 7). Notes that the response of streamflow follows the response of precipitation and evapotranspiration.

The effect of deforestation causes an increase in streamflow during the rainy season (DJF) in normal conditions (December 1985 and January and February 1986) and especially under the La Niña event (December 1988 and January and February 1989) in all sub-basins, except in SB7, sub-basin that has the largest deforested area (Fig. 8a). During the acting of El Niño (December 1986 and January and February 1987, and December 1987 and January and February 1988), the effect of LUCC is of reduction in streamflow in all sub-basins in the rainy season (Fig. 8a). Notably, this reduction is greater at the end of El Niño, probably due to hydrological memory.

In the dry season, the effect of LUCC on streamflow is of decrease in both El Niño and La Niña in all sub-basins (Fig. 8b). Notes that this reduction in streamflow at the beginning of La Niña is higher than in the El-Niño periods. This result could have the signature of the dry memory of the last years when El Niño occurred.

Thus, as expected, changes in the streamflow driven by the conversion from forest to pasture in the experiments are highly modulated by the changes in the evapotranspiration

because of differences in plant physiology and changes in precipitation induced by the surface heterogeneity and the coupling with the atmosphere.

## 4 Discussions and conclusions

The 1-km version of the Eta/Noah-MP model was used to simulate the local hydroclimatic response to land-use and land cover changes over southeastern Rondonia, including the Ji-Parana basin, between 1984 and 1989, when the annual deforestation rates in the region were the highest ever recorded (Linhares 2005). For this purpose, two experiments were set up, one control without changes in land use and another changing land use annually.

Precipitation is affected by land use changes, showing stronger impacts where deforestation was expanded over the years studied. Higher precipitation volumes simulated by the CTL experiment over forested lands in the rainy season are reduced with the increase of deforestation in the LUCC experiment.

In August, the driest month in the region, there is an increase in precipitation of up to  $3 \text{ mm day}^{-1}$  with the growth of deforestation. Some previous studies found that the fish-bone fragmentation in Ji-Parana triggers mesoscale circulations leading to an increase in shallow cumulus clouds and convective precipitation during dry periods (e.g., Baidya Roy 2009; Khanna et al. 2017; Negri et al. 2004; Wang et al. 2009). Therefore, our results suggest that increased precipitation in dry periods over pasture lands could be associated with circulations induced by surface heterogeneities.

An increase in deforestation reduces evapotranspiration and the net radiation at the surface, increasing the near-surface air temperature and sensible heat flux in the dry season. This behavior agrees with previous studies using global and regional models and observational data (e.g., Baidya Roy 2009; Sampaio et al. 2007; von Randow et al. 2004).

In the rainy season, the simulated response to LUCC shows an increase in evapotranspiration over some areas, where occurred expansion of pasture lands. During the wet season, evapotranspiration increases in pasture areas because of the larger water availability in the shallow root zone associated with higher precipitation volumes. Stomatal resistance is lower in pasture areas than in the forest, contributing to increased evaporation in deforested regions under wet conditions (Pilotto et al. 2017). This increase in evapotranspiration cools the air near the surface, which decreases the sensible heat flux and the longwave radiation emitted by the surface, increasing the net radiation.

Notes that the impacts of LUCC on high-resolution simulations of the near-surface air temperature and the energy

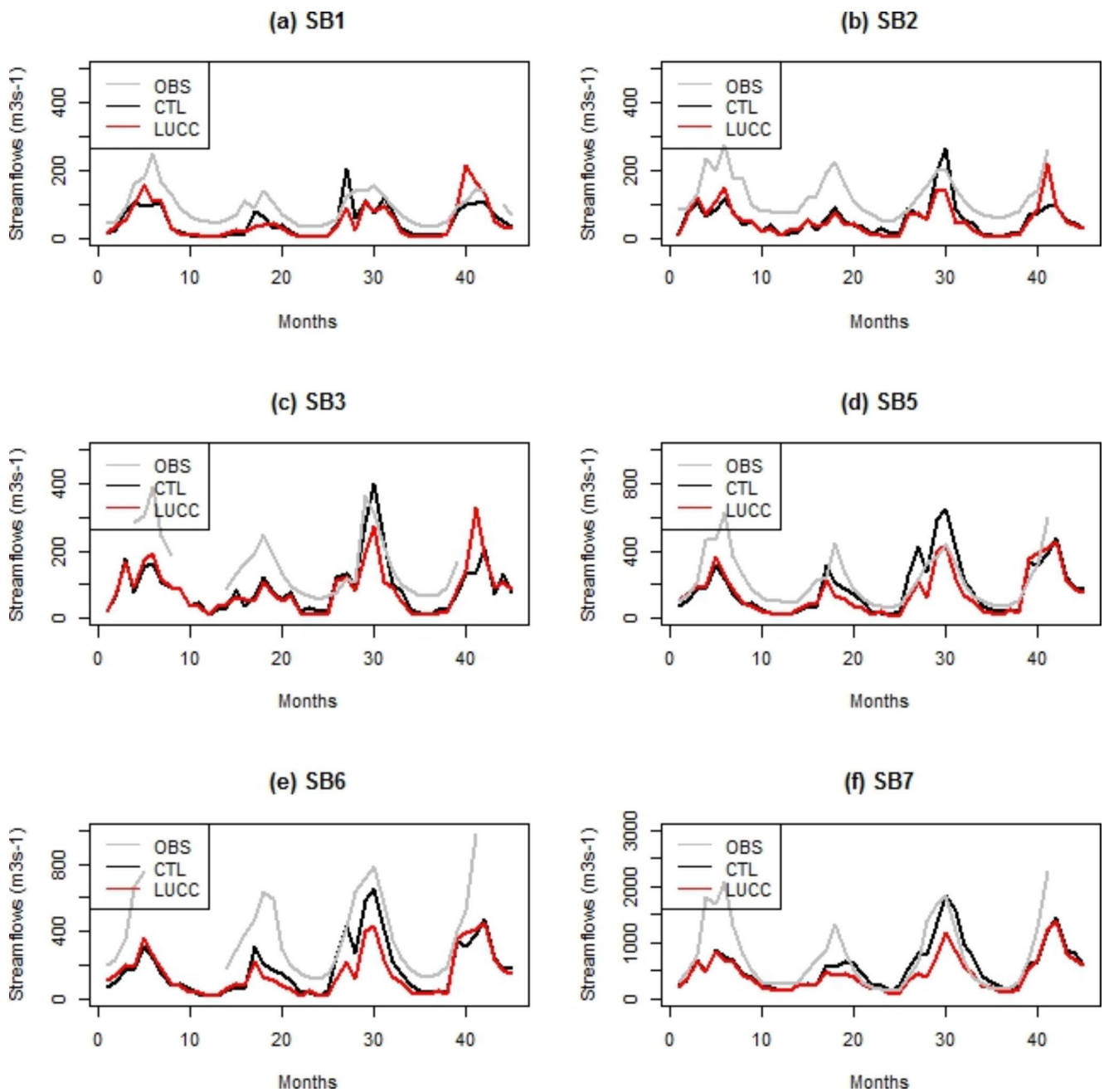


**Fig. 7** Monthly streamflow ( $\text{m}^3\text{s}^{-1}$ ) from the (black curves) CTL and (red curves) LUCC experiments and (grey curves) observed in (a,b,c,d,e,f) seven sub-basins of Ji-Parana, except in the sub-basin four due to observed data failures

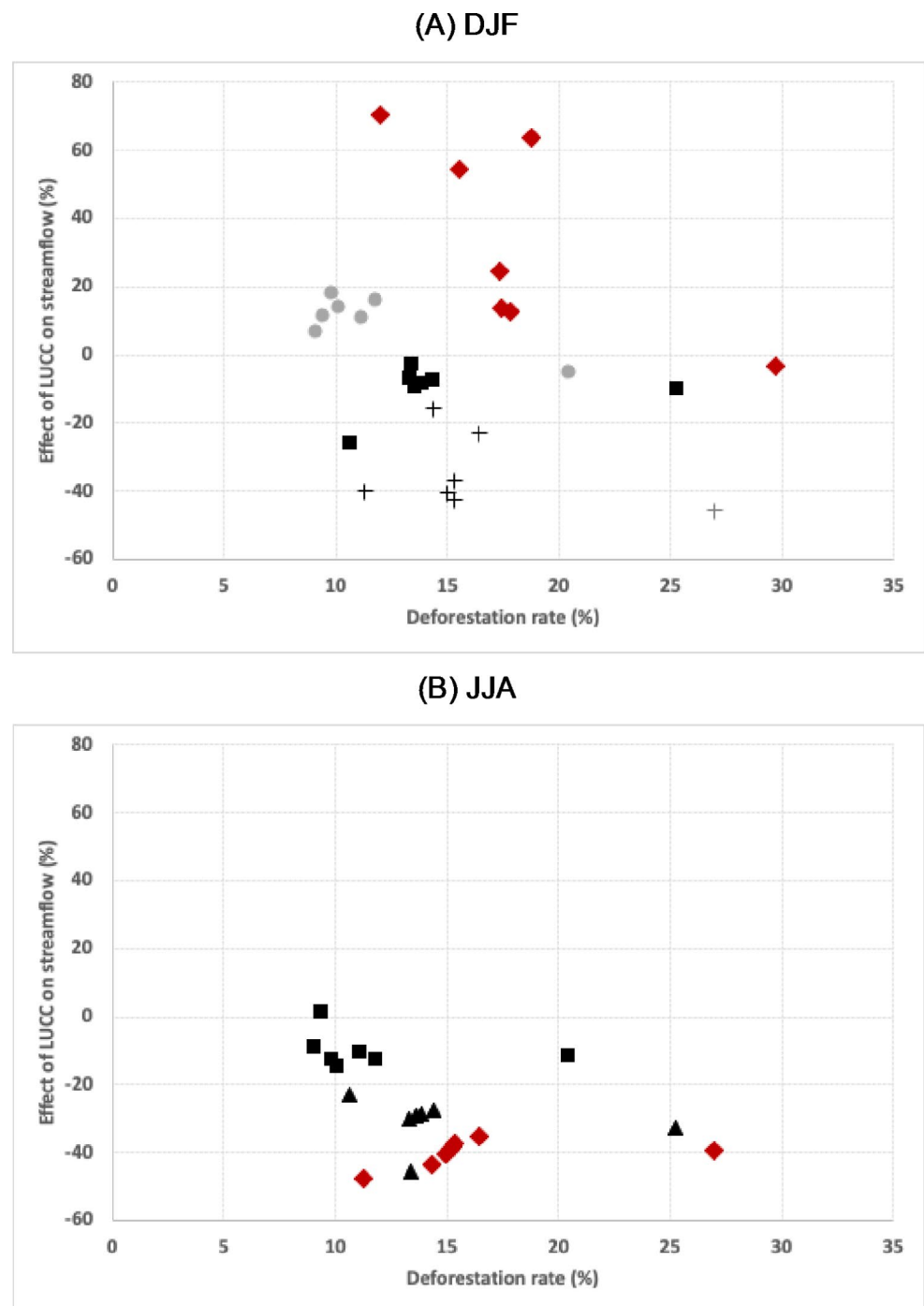
**Table 1**  $R^2$  and RMSE values of monthly streamflows from the CTL and LUCC experiments in sub-basin 1 (SB1), 2 (SB2), 3 (SB3), 5 (SB5), 6 (SB6), 7 (SB7)

Monthly	$R^2$		RMSE	
	CTL	LUCC	CTL	LUCC
SB1	0.55	0.53	54.23	56.74
SB2	0.44	0.67	82.30	79.80
SB3	0.53	0.71	93.30	96.00
SB5	0.45	0.60	131.67	122.71
SB6	0.59	0.64	237.63	270.40
SB7	0.56	0.75	441.12	504.16

fluxes are distributed over the fishbone and large proprieties patches typical of the region, mainly during the dry season.

Interannual variability indicates that the large differences between the experiments occur in years influenced by extreme precipitation events (El Niño and La Niña). This result suggests that LUCC may intensify the impacts on precipitation caused by El Niño/La Niña events. The land use change between 1983 and 1984, with an annual deforestation rate of almost 10%, produces small local hydrometeorological changes. However, these results show

**Fig. 8** Scatter plotter of deforestation rate in Ji-Parana Basin (%) versus the effect of LUCC on streamflow (LUCC-CTL/CTL) (%) for (a) DJF and (b) JJA. In DJF, the gray circle corresponds to 1985 and 1986, the black square is 1986 and 1987, the black cross is 1987 and 1988, and the red diamond is 1988 and 1989. In JJA, the black square corresponds to 1986, the black triangle is 1987, and the red diamond is 1988



that interannual climate variability enhances the impacts of LUCC on the local hydroclimate in the Ji-Parana basin. Indeed, even with the very high annual deforestation rate, the percentage of deforested areas in 1984 was 17% over the Ji-Parana Basin, below the percentages of more recent decades that exceed 50%. Therefore, it is suggested that for deforested areas below 20–30%, large-scale climatic effects interfere more with the local climate than land use changes.

One hypothesis to explain the reduction in rainfall with the increased deforestation is that during the El Niño there is less availability of water vapor in the atmosphere in the region. Additionally, the removal of the forests reduces evapotranspiration, further decreasing the amount of water vapor available in the atmosphere, and consequently of the precipitation. While the increase in rainfall during La Niña could be associated with the same process that occurs when the pasture evapotranspires more than the forest in wetter

periods (e.g., Pilotto et al. 2017). Lee and Lo (2021) found an increase in precipitation in deforestation experiments during El Niño periods. Our study region, located in the southern Amazon, exhibits continental characteristics. The Amazon rainforest has high rates of precipitation recycling through forest evapotranspiration. However, during El Niño events, there is a likelihood of reduced precipitation in the region during the wet season (Cai et al. 2020). Additionally, under deforestation scenarios, evapotranspiration is significantly reduced, leading to a decrease in available water for precipitation.

Coupled atmosphere, land surface, and channel routing integrations allow the analyses of feedback impacts on the hydrological response of the basin under land use change. Despite the model limitations, it is possible to evaluate compensatory mechanisms between changes in evapotranspiration and precipitation driven by the land use change dynamic. Land-use changes reduce the streamflow in all sub-basins of Ji-Parana during the dry season. In the rainy season, LUCC increases the streamflow during periods with normal precipitation conditions, especially in the La Niña years, in almost all sub-basins except in the sub-basin that is more deforested, where soil moisture availability allows large evapotranspiration rates from pasture.

**Supplementary Information** The online version contains supplementary material available at <https://doi.org/10.1007/s00382-023-06872-x>.

**Acknowledgements** This study was financed in part by the Coordenação de Aperfeiçoamento de Pessoal de Nível Superior – Brasil – Agência Nacional de Águas (CAPES-ANA) - Finance Code 88887.115869/2015-01. The authors thank the São Paulo Research Foundation (FAPESP) Grant 2014/50848-9 and Grant 2018/02982-9, the National Council for Scientific and Technological Development (CNPq) Grant 308358/2018-0, the National Institute of Science and Technology for Climate Change Phase 2 under CNPq Grant 465501/2014-1, the CAPES Grant 16/2014, and the CNPq-ANA Grant 446197/2015-7.

**Author contributions** All authors contributed to the study's conception and design. Material preparation and data collection were performed by Isabel L. Pilotto. Analysis was performed by Isabel L. Pilotto and Daniel A. Rodriguez. The first draft of the manuscript was written by Isabel L. Pilotto and all authors commented on previous versions of the manuscript. All authors read and approved the final manuscript.

**Funding** This work was supported by the Coordenação de Aperfeiçoamento de Pessoal de Nível Superior – Brasil – Agência Nacional de Águas (CAPES-ANA) – Grant number 88887.115869/2015-01.

**Data Availability** The datasets generated during the current study are not publicly available due to lack of structure and resources but are available from the corresponding author on reasonable request.

## Declarations

**Competing interests** The authors declare no competing interests.

**Ethical approval** Not applicable.

**Competing interests** The authors have no relevant financial or non-financial interests to disclose.

## References

- Aceituno P (1988) On the functioning of the southern oscillation in the South American sector: surface, climate. *Mon Weather Rev* 116:505–524
- Almeida CAD, Coutinho AC, Esquerdo JCDM, Adami M, Venturieri A, Diniz CG, Dessay N, Durieux L, Gomes AR (2016) High spatial resolution land use and land cover mapping of the Brazilian Amazon in 2008 using Landsat-5/TM and MODIS data. *Acta Amaz* 46:291–302
- Alves DS (2002a) An analysis of the geographical patterns of deforestation in the Brazilian Amazon in the period 1991–1996. *Deforestation and land use in the Amazon* 95–106
- Alves DS (2002b) Space–time dynamics of deforestation in Brazilian Amazon. *Int J Remote Sens* 23:2903–2908
- Alves DS, Pereira JLG, De Sousa CL, Soares JV, Yamaguchi F (1999) Characterizing landscape changes in central Rondonia using Landsat TM imagery. *Int J Remote Sens* 20:2877–2882. <https://doi.org/10.1080/014311699211859>
- Alves DS, Escada M, Pereira J, Linhares C (2003) Land use intensification and abandonment in Rondônia. *Int J Remote Sens* 24:899–903
- Arima EY, Walker RT, Perz S, Souza C (2016) Explaining the fragmentation in the Brazilian Amazon forest. *J Land Use Sci* 11:257–277. <https://doi.org/10.1080/1747423X.2015.1027797>
- Baidya Roy S (2009) Mesoscale vegetation–atmosphere feedbacks in Amazon. *J Geophys Res* 114:D20111. <https://doi.org/10.1029/2009JD012001>
- Baidya Roy S, Avissar R (2002) Impact of land use/land cover change on regional hydrometeorology in Amazon. *J Phys Res* 107(D20):1–12. <https://doi.org/10.1029/2000JD000266>
- Beck HE, van Dijk AIJM, Levizzani V, Schellekens J, Miralles DG, Martens B, de Roo A (2017) MSWEP: 3-hourly 0.25° global gridded precipitation (1979–2015) by merging gauge, satellite, and reanalysis data. *Hydrol Earth Syst Sci* 21:589–615. <https://doi.org/10.5194/hess-21-589-2017>
- Bruno R, da Rocha HR, de Freitas HC, Goulden ML, Miller SD (2006) Soil moisture dynamics in an eastern Amazon tropical forest. *Hydrol Process* 20:2477–2489
- Cai W, McPhaden MJ, Grimm AM et al (2020) Climate impacts of the El Niño–Southern Oscillation on South America. *Nat Rev Earth Environ* 1:215–231. <https://doi.org/10.1038/s43017-020-0040-3>
- Chagnon FJF, Bras RL (2005) Contemporary climate change in the Amazon. *Geophys Res Lett* 32(13):1–4. <https://doi.org/10.1029/2005GL022722>
- Chagnon FJF, Bras RL, Wang J (2004) Climatic shift in patterns of shallow clouds over the Amazon. *Geophys Res Lett*. <https://doi.org/10.1029/2004GL021188>
- Chen F, Janjić Z, Mitchell K (1997) Impact of atmospheric surface-layer parameterizations in the new land-surface scheme of the NCEP mesoscale Eta model. *Boundary Layer Meteorol* 85(3):391–421. <https://doi.org/10.1023/A:1000531001463>
- Chou SC, Bustamante JF, Gomes JL (2005) Evaluation of Eta Model seasonal precipitation forecasts over South America. *Nonlinear Process Geophys* 12(4):537–555. <https://doi.org/10.5194/npg-12-537-2005>
- Chou SC, Marengo JA, Lyra A, Sueiro G, Pesquero J, Alves LM, Kay G, Betts R, Chagas D, Gomes JL, Bustamante J, Tavares P (2012) Downscaling of South America present climate driven

- by 4-member HadCM3 runs. *Clim Dyn* 38(3–4):635–653. <https://doi.org/10.1007/s00382-011-1002-8>
- Chou SC, Lyra A, Mourão C, Dereczynski C, Pilotto I, Gomes J, Bustamante J, Tavares P, Silva A, Rodrigues D, Campos D, Chagas D, Sueiro G, Siqueira G, Marengo J (2014) Assessment of Climate Change over South America under RCP 4.5 and 8.5 downscaling scenarios. *Am J Clim Change* 03(05):512–527. <https://doi.org/10.4236/ajcc.2014.35043>
- Chou, Nunes et al (2019) Springer Nature
- Correia FWS, Alvalá RCS, Manzi AO (2008) Modeling the impacts of land cover change in Amazon: a regional climate model (RCM) simulation study. *Theoret Appl Climatol* 93(3–4):225–244. <https://doi.org/10.1007/s00704-007-0335-z>
- Costa MH, Foley JA (2000) Combined effects of deforestation and doubled atmospheric CO<sub>2</sub> concentrations on the climate of Amazon. *J Clim* 13(1):18–34. [https://doi.org/10.1175/15200442\(2000\)013%3C0018:CEODAD%3E2.0.CO;2](https://doi.org/10.1175/15200442(2000)013%3C0018:CEODAD%3E2.0.CO;2)
- Cunge JA (1969) On the subject of the flood propagation computation method. *J Hydraul Res* 7:205–230
- D’Almeida C, Vörösmarty CJ, Hurr G, Marengo JA, Dingman SL, Keim BD (2007) The effects of deforestation on the hydrological cycle in Amazon: a review on scale and resolution. *Int J Climatol* 633–647
- da Rocha HR, Goulden ML, Miller SD, Menton MC, Pinto LDVO, de Freitas HC, Silva Figueira AM (2004) Seasonality of water and heat fluxes over a tropical forest in eastern Amazonia. *Ecol Appl* 14:22–32. <https://doi.org/10.1890/02-6001>
- da Silva RR, Werth D, Avissar R (2008) Regional impacts of future land-cover changes on the Amazon basin wet-season climate. *J Clim* 21(6):1153–1170. <https://doi.org/10.1175/2007JCLI1304.1>
- de Oliveira Filho FJB, Metzger JP (2006) Thresholds in landscape structure for three common deforestation patterns in the Brazilian Amazon. *Landscape Ecol* 21(7):1061–1073. <https://doi.org/10.1007/s10980-006-6913-0>
- Dee DP, Uppala SM, Simmons AJ, Berrisford P, Poli P, Kobayashi S, Andrae U, Balmaseda MA, Balsamo G, Bauer P, Bechtold P, Beljaars ACM, van de Berg L, Bidlot J, Bormann N, Delsol C, Dragani R, Fuentes M, Geer AJ, Haimberger L, Healy SB, Hersbach H, H??lm EV, Isaksen L, K??llberg P, K??hler M, Matricardi M, McNally AP, Monge-Sanz BM, Morcrette JJ, Park BK, Peubey C, de Rosnay P, Tavolato C, Th??paut JN, Vitart F (2011) The ERA-Interim reanalysis: configuration and performance of the data assimilation system. *Q J R Meteorol Soc* 137(656):553–597. <https://doi.org/10.1002/qj.828>
- Dijkshoorn JA, Huting JRM, Tempel P (2005) Update of the 1:5 million Soil and Terrain Database for Latin America and the Caribbean (SOTERLAC; version 2.0), Report 2005/01, ISRIC – World Soil Information, Wageningen, Netherlands
- Ek MB, Mitchell KE, Lin Y, Rogers E, Grunmann P, Koren V, Gayno G, Tarpley JD (2003) Implementation of Noah land surface model advances in the National Centers for Environmental Prediction operational mesoscale Eta model. *J Geophys Research: Atmos* 108(D22). <https://doi.org/10.1029/2002JD003296>
- Espinoza JC et al (2012) From drought to flooding: understanding the abrupt 2010–2011 hydrological annual cycle in the Amazonas River and tributaries. *Environ Res Lett* 7:024008
- Espinoza JC, Ronchail J, Frappart F, Lavado W, Santini W, Guyot JL (2013) The major floods in the Amazonas river and tributaries (western Amazon basin) during the 1970–2012 period: a focus on the 2012 flood. *J Hydrometeorol* 14:1000–1008
- Farr TG, Kobrick M (2000) Shuttle Radar Topography Mission produces a wealth of data. *EOS (Transactions American Geophysical Union)* 81:583–585
- Farr TG et al (2007) The Shuttle Radar Topography Mission. *Review of Geophysics* 45: RG2004
- Fels SB, Schwarzkopf MD (1975) The Simplified Exchange Approximation: a New Method for Radiative transfer calculations. *J Atmos Sci* 32(7):1475–1488. [https://doi.org/10.1175/1520-0469\(1975\)032%3C1475:TSEAA%3E2.0.CO;2](https://doi.org/10.1175/1520-0469(1975)032%3C1475:TSEAA%3E2.0.CO;2)
- Findell KL, Shevliakova E, Milly PCD, Stouffer RJ (2007) Modeled impact of anthropogenic land cover change on climate. *J Clim* 20(14):3621–3634. <https://doi.org/10.1175/JCLI4185.1>
- Guillod BP, Orlovsky B, Miralles DG, Teuling AJ, Seneviratne SI (2015) Reconciling spatial and temporal soil moisture effects on afternoon rainfall. *Nat Commun* 6. <https://doi.org/10.1038/ncomms7443>
- Harmel RD, Veith TL, Arnold JG, Van Liew MW, Bingner RL, Moriasi DN (2007) Model evaluation guidelines for systematic quantification of Accuracy in Watershed Simulations. *Trans ASABE* 50(3):885–900. <https://doi.org/10.13031/2013.23153>
- Imbach P, Chou SC, Lyra A, Rodrigues D, Rodriguez D, Latinovic D et al (2018) Future climate change scenarios in Central America at high spatial resolution. *PLoS ONE* 13(4):e0193570. <https://doi.org/10.1371/journal.pone.0193570>
- Instituto Nacional de Pesquisas Espaciais – INPEa, Coordenação Geral de Observação da Terra – OBT (2022) ‘Projeto PRODES: monitoramento da Floresta Amazônica Brasileira por Satélite’. <http://www.obt.inpe.br/prodes> (accessed 18 March 2022)
- Instituto Nacional de Pesquisas Espaciais – INPEb, Coordenação Geral de Observação da Terra – OBT (2022) ‘Projeto TerraClass: Mapeamento do Uso e Cobertura da Terra na Amazônia Legal Brasileira’. [http://www.inpe.br/cra/projetos\\_pesquisas/dados\\_terraclass.php](http://www.inpe.br/cra/projetos_pesquisas/dados_terraclass.php) (accessed 18 March 2022)
- Instituto Nacional de Meteorologia – INMET (1992) Normais Climatológicas (1961–1990). INMET – Instituto Nacional de Meteorologia/Ministério da Agricultura e Reforma Agrária: Brasília
- Janjić ZI (1994) The step-mountain Eta Coordinate Model: further developments of the Convection, Viscous Sublayer, and Turbulence Closure Schemes. *Mon Weather Rev* 927–945
- Jarvis PG, Series B (1976) Biological Sciences The Royal Society Phil. Trans R Soc Lond B 273(273): 593–610
- Khanna J, Medvigy D, Fueglistaler S, Walko R (2017) Regional dry-season climate changes due to three decades of Amazon deforestation. *Nat Clim Change* 7(3):200–204. <https://doi.org/10.1038/nclimate3226>
- Koster RD, Dirmeyer PA, Guo Z, Bonan G, Chan E, Cox P, Gordon CT, Kanae S, Kowalczyk E, Lawrence D, Liu P, Lu CH, Malyshev S, McAvaney B, Mitchell K, Mocko D, Oki T, Oleson K, Pitman A, Sud YC, Taylor CM, Verseghy D, Vasic R, Xue Y, Yamada T (2004) Regions of strong coupling between soil moisture and precipitation. *Science* 305:1138–1140. <https://doi.org/10.1126/science.1100217>
- Lacis A, Hansen J (1974) A parameterization for the absorption of Solar Radiation in the Earth’s atmosphere. *J Atmos Sci* 118–133
- Lee T-H, Lo M-H (2021) The role of El Niño in modulating the effects of deforestation in the Maritime Continent. *Environ Res Lett* 16. <https://doi.org/10.1088/1748-9326/abe88e>
- Lejeune Q, Davin EL, Guillod BP, Seneviratne SI (2015) Influence of Amazon deforestation on the future evolution of regional surface fluxes, circulation, surface temperature and precipitation. *Clim Dyn* 44(9–10):2769–2786. <https://doi.org/10.1007/s00382-014-2203-8>
- Linhares C (2005) Influência do Desflorestamento na Dinâmica da Resposta Hidrológica na Bacia do Rio Ji-Paraná/RO. *Thesis*
- Lyra A, Tavares P, Chou SC, Sueiro G, Dereczynski C, Sondermann M, Silva A, Marengo J, Giarolla A (2018) Climate change projections over three metropolitan regions in Southeast Brazil using the non-hydrostatic Eta regional climate model at 5-km resolution. *Theoret Appl Climatol* 132(1–2):663–682. <https://doi.org/10.1007/s00704-017-2067-z>

- Machado LA (1998) A fronteira agrícola na Amazônia brasileira. In *Geografia e Meio Ambiente no Brasil*, edited by B. K. Becker, A. Christofletti, F. R. Davidovich and P. R. Geiger, 2nd edn (São Paulo: Hucitec), pp. 181–217
- Marengo JA, Espinoza JC (2016) Extreme seasonal droughts and floods in Amazonia: causes, trends and impacts. *Int J Climatol* 36:1033–1050. <https://doi.org/10.1002/joc.4420>
- Marengo JA, Chou SC, Kay G, Alves L, Pesquero JF, Soares WR, Santos DC, Lyra AA, Sueiro G, Betts R, Chagas DJ, Gomes JL, Bustamante JF, Tavares P (2012) Development of regional future climate change scenarios in South America using the Eta CPTec/HadCM3 climate change projections: climatology and regional analyses for the Amazon, São Francisco and the Parana River basins. *Clim Dyn* 38(9–10):1829–1848. <https://doi.org/10.1007/s00382-011-1155-5>
- Medvigy D, Walko RL, Avissar R (2011) Effects of Deforestation on Spatiotemporal Distributions of Precipitation in South America. *J Clim* 24(8):2147–2163. <https://doi.org/10.1175/2010JCLI3882.1>
- Mellor GL, Yamada T (1982) Development of a turbulence closure model for geophysical fluid problems. *Reviews of Geophysical Physics and Space Physics* 20:851–875
- Mesinger F (1984) A blocking technique for representation of mountains in atmospheric models. *Rivista di Meteorologia Aeronautica* 44:195–202
- Mesinger F, Chou SC, Gomes JL, Jovic D, Bastos P, Bustamante JF, Lazic L, Lyra AA, Morelli S, Ristic I, Veljovic K (2012) An upgraded version of the Eta model. *Meteorol Atmos Phys* 116(3–4):63–79. <https://doi.org/10.1007/s00703-012-0182-z>
- Negri AJ, Adler RF, Xu L, Surratt J (2004) The impact of Amazon deforestation on dry season rainfall. *J Clim* 17(6):1306–1319. [https://doi.org/10.1175/1520-0442\(2004\)017%3C1306:TIOADO%3E2.0.CO;2](https://doi.org/10.1175/1520-0442(2004)017%3C1306:TIOADO%3E2.0.CO;2)
- Niu GY, Yang ZL (2004) Effects of vegetation canopy processes on snow surface energy and mass balances. *J Geophys Res D: Atmos* 109(23):1–15. <https://doi.org/10.1029/2004JD004884>
- Niu GY, Yang ZL, Dickinson RE, Gulden LE (2005) A simple TOP-MODEL-based runoff parameterization (SIMTOP) for use in global climate models. *J Geophys Res Atmos* 110(21):1–15. <https://doi.org/10.1029/2005JD006111>
- Niu G-Y, Yang Z-L, Dickinson RE, Gulden LE, Su H (2007) Development of a simple groundwater model for use in climate models and evaluation with gravity recovery and climate experiment data. *J Geophys Res* 112. <https://doi.org/10.1029/2006JD007522>
- Niu GY, Yang ZL, Mitchell KE, Chen F, Ek MB, Barlage M, Kumar A, Manning K, Niyogi D, Rosero E, Tewari M, Xia Y (2011) The community Noah land surface model with multiparameterization options (Noah-MP): 1. Model description and evaluation with local-scale measurements. *J Geophys Res Atmos* 116(12):1–19. <https://doi.org/10.1029/2010JD015139>
- Nobre C, Sellers PJ, Shukla J (1991) Amazon Deforestation and Regional Climate Change. *J Clim* 9:957–988
- Pesquero JF, Chou SC, Nobre CA, Marengo JA (2010) Climate downscaling over South America for 1961–1970 using the Eta Model. *Theoret Appl Climatol* 99:75–93. <https://doi.org/10.1007/s00704-009-0123-z>
- Pilotto IL, Chou SC, Nobre P (2012) Seasonal climate hindcasts with Eta model nested in CPTec coupled ocean-atmosphere general circulation model. *Theoret Appl Climatol* 110(3):437–456. <https://doi.org/10.1007/s00704-012-0633-y>
- Pilotto IL, Rodríguez DA, Tomasella J, Sampaio G, Chou SC (2015) Comparisons of the Noah-MP land surface model simulations with measurements of forest and crop sites in Amazon. *Meteorology and Atmospheric Physics*. Springer Vienna 127(6):711–723. <https://doi.org/10.1007/s00703-015-0399-8>
- Pilotto IL, Rodríguez DA, Chan Chou S, Tomasella J, Sampaio G, Gomes JL (2017) Effects of the surface heterogeneities on the local climate of a fragmented landscape in Amazon using a tile approach in the Eta/Noah-MP model. *Q J R Meteorol Soc* 143(704):1565–1580. <https://doi.org/10.1002/qj.3026>
- Pitman AJ, Lorenz R (2016) Scale dependence of the simulated impact of Amazon deforestation on regional climate. *Environ Res Lett* 11(9). <https://doi.org/10.1088/1748-9326/11/9/094025>
- Resende NC, Miranda JH, Cooke R, Chu ML, Chou SC (2019) Impacts of regional climate change on the runoff and root water uptake in corn crops in Parana, Brazil. *Agric Water Manage* 221:556–565. <https://doi.org/10.1016/j.agwat.2019.05.018>
- Rodriguez DA, Tomasella J (2016) On the ability of large-scale hydrological models to simulate land use and land cover change impacts in Amazon basins. *Hydrol Sci J* 61(10):1831–1846. <https://doi.org/10.1080/02626667.2015.1051979>
- Rodriguez DA, Tomasella J, Linhares C (2010) Is the forest conversion to pasture affecting the hydrological response of Amazon catchments? Signals in the Ji-Paraná Basin. *Hydrol Process* 24(10):1254–1269. <https://doi.org/10.1002/hyp.7586>
- Rodriguez DA, Chou SC, Tomasella J, Demaria EMC (2014) Impacts of landscape fragmentation on simulated precipitation fields in the Amazon sub-basin of Ji-Paraná using the Eta model. *Theoret Appl Climatol* 115(1–2):121–140. <https://doi.org/10.1007/s00704-013-0866-4>
- Sampaio G, Nobre C, Costa MH, Satyamurty P, Soares-Filho BS, Cardoso M (2007) Regional climate change over eastern Amazonia caused by pasture and soybean cropland expansion. *Geophys Res Lett* 34:L17709. <https://doi.org/10.1029/2007GL030612>
- Seneviratne SI, Lüthi D, Litschi M, Schär C (2006) Land-atmosphere coupling and climate change in Europe. *Nature* 443:205–209. <https://doi.org/10.1038/nature05095>
- Tavares PS, Giarolla A, Chou SC, Silva AJP, Lyra AA (2018) Climate change impact on the potential yield of Arabica coffee in southeast Brazil. *Reg Environ Change* (2017) 18: 873
- Uvo CB, Repelli C, Zebiak S, Kushnir Y (1998) The relationship between tropical Pacific and Atlantic SST and northeast Brazil monthly precipitation. *J Clim* 11:551–562
- von Randow C, Manzi AO, Kruijt B, de Oliveira PJ, Zanchi FB, Silva RL, Hodnett MG, Gash JHC, Elbers JA, Waterloo MJ, Cardoso FL, Kabat P (2004) Comparative measurements and seasonal variations in energy and carbon exchange over forest and pasture in South West Amazon. *Theoret Appl Climatol* 78(1–3):5–26. <https://doi.org/10.1007/s00704-004-0041-z>
- Wang J, Bras RL, Eltahir EB (2000) The impact of observed Deforestation on the Mesoscale distribution of Rainfall and Clouds in Amazon. *J Hydrometeorol* 1(3):267–286. [https://doi.org/10.1175/1525-7541\(2000\)001%3C0267:TIOODO%3E2.0.CO;2](https://doi.org/10.1175/1525-7541(2000)001%3C0267:TIOODO%3E2.0.CO;2)
- Wang J, Chagnon FJF, Williams ER, Betts AK, Renno NO, Machado LAT, Bisht G, Knox R, Bras RL (2009) Impact of deforestation in the Amazon basin on cloud climatology. *Proc Natl Acad Sci* 106(10):3670–3674. <https://doi.org/10.1073/pnas.0810156106>
- Williams E, Dall’Antonia A, Dall’Antonia V, de Almeida J, Suarez F, Liebmann B, Malhado ACM (2005) The drought of the century in the Amazon basin: an analysis of the regional variation of rainfall in South America in 1926. *Acta Amazonia* 35(2):231–238. <https://doi.org/10.1590/S0044-59672005000200013>
- Yang RQ, Friedl MA (2003) Modeling the effects of three-dimensional vegetation structure on surface radiation and energy balance in boreal forests. *J Geophys Research-Atmospheres* 108. <https://doi.org/10.1029/2002jd003109>
- Zhang R-H, Endoh M (1994) Simulation of the 1986–87 El Niño and 1988 La Niña events with a free surface tropical Pacific OGCM. *J Geophys Res* 99:7743–7759

Zhao Q, Carr FH (2002) A Prognostic Cloud Scheme for operational NWP models. *Mon Weather Rev* 125(8):1931–1953. [https://doi.org/10.1175/1520-0493\(1997\)125%3C1931:apcsfo%3E2.0.co;2](https://doi.org/10.1175/1520-0493(1997)125%3C1931:apcsfo%3E2.0.co;2)

**Publisher's Note** Springer Nature remains neutral with regard to jurisdictional claims in published maps and institutional affiliations.

Springer Nature or its licensor (e.g. a society or other partner) holds exclusive rights to this article under a publishing agreement with the author(s) or other rightsholder(s); author self-archiving of the accepted manuscript version of this article is solely governed by the terms of such publishing agreement and applicable law.